X-ray and Raman scattering study of orientational order in nematic and heliconical nematic liquid crystals

Gautam Singh, Jinxin Fu, Dena M. Agra-Kooijman, Jang-Kun Song, M. R. Vengatesan, Mohan Srinivasarao, Michael R. Fisch, and Satyendra Kumar

Phys. Rev. E **94**, 060701 — Published 13 December 2016

DOI: 10.1103/PhysRevE.94.060701

X-ray and Raman Scattering Study of Orientational Order in the Nematic and Heliconical Nematic Liquid Crystals

Gautam Singh,[a,c] Jinxin Fu,[d] Dena M. Agra-Kooijman,[a] Jang-Kun Song,[e] M. R. Vengatesan,[e] Mohan Srinivasarao,[d] Michael R. Fisch,[b] and Satyendra Kumar [a,f]

[a]Department of Physics and [b]College of Applied Engineering Sustainability and Technology
Kent State University, Kent, OH 44242

[c]Department of Applied Physics, AIAS, Amity University, Noida, India

[d]School of Materials Science and Engineering, School of Chemistry and Biochemistry, and
Center for Advanced Research on Optical Microscopy,
Georgia Institute of Technology, Atlanta GA 30332-0295

[e]School of Electronic and Electrical Engineering, Sungkyunkwan University
Suwon, Republic of Korea

[f]Division of Research and Department of Physics, University at Albany, Albany, NY 12222

Abstract

The temperature dependence of the orientational order parameters, $\langle P_2(\cos\beta)\rangle$ and $\langle P_4(\cos\beta)\rangle$ in the nematic (*N*) and twist-bend nematic (N_{tb}) phases of the liquid crystal dimer CB7CB have been measured using x-ray and polarized Raman scattering. The $\langle P_2(\cos\beta)\rangle$ obtained from both techniques are the same; while $\langle P_4(\cos\beta)\rangle$, determined by Raman scattering is, as expected, systematically larger than its x-ray value. Both order parameters increase in the N phase with decreasing temperature, drop across the N - N_{tb} transition, and continues to decrease. In the N_{tb} phase, the x-ray value of $\langle P_4(\cos\beta)\rangle$ eventually becomes negative providing a direct and independent confirmation of a conical molecular orientational distribution. The heliconical tilt angle, α, determined from orientational distribution functions in the N_{tb} phase increases to ~24° at ~ 15 K below the transition. In the N_{tb} phase, $\alpha(T) \propto (T^* - T)^{\lambda}$, $\lambda = 0.19 \pm 0.03$. The transition supercools by 1.7 K, consistent with its weakly first order nature. The value of λ is close to 0.25 indicating close proximity to a tricritical point.

PACS Numbers: 61.30.Gd, 61.30.Eb, 64.70.mj

Corresponding author: mfisch@kent.edu

The *nematic* (N) phase is the most widely studied liquid crystal phase and is used in the ubiquitous flat panel displays and other electrooptical applications. This phase is characterized [1] by long-range orientation order of the molecules' symmetry axis along the *director* (a pseudo-vector) ***n***, as shown in Fig. 1(a). When the molecules are chiral (i.e., lack mirror symmetry), the *cholesteric* phase is obtained. Here, the local ***n*** describes a helical trajectory, Fig. 1(b), in a direction perpendicular to itself. Recently, a very different kind of chiral nematic phase was discovered in systems of calamitic bent-shape bimesogens. It differs from the previously known cholesteric phase in that the local director ***n*** precesses about the helical axis ***N*** at an oblique angle α [Fig. 1(c)] and lies on the surface of a cone. This heliconical phase is called the *twist-bend nematic* (N_{tb}) phase and is known to be a consequence of a negative bend elastic constant. Although the N_{tb} phase was originally predicted on the basis of theoretical considerations [2] and simulations [3] for bent-core (or, banana-shape) molecules, it was first discovered in calamitic bimesogens [4, 5, 6] and then in two systems of bent-core (banana-shaped) molecules by the Clark [7] and Kumar [8] groups.

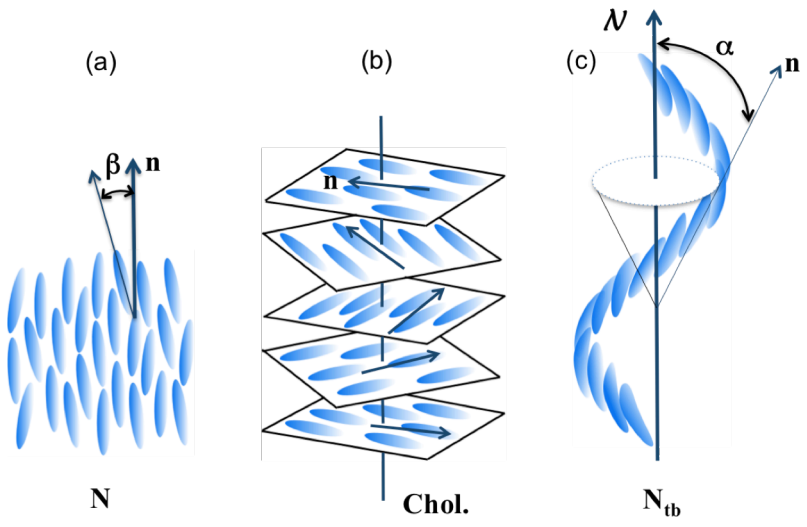

Figure 1: Schematic representation of the (a) calamitic nematic, **N**; (b) cholesteric, **Chol.** and (c) twist-bend nematic $\mathbf{N_{tb}}$ phases of a molecule with bent shape. Here, arrows with **n** represent the local director while ***N*** is the global director.

All known calamitic dimers exhibiting the N_{tb} phase consist of two mesogenic units linked by a flexible spacer of an odd number of hydrocarbons that give the molecule a bent conformation. For example, two cyanobiphenyl (CB) moieties linked by alkyl chains of three, five, or seven hydrocarbon moieties (*e.g.*, 1″,7″-bis(4-cyanobiphenyl-4′-yl) heptane, CB7CB, has two CB moieties connected by seven methylenes) exhibit the N-N_{tb} transition, while the same set of moieties linked with even number of methylenes exhibit no such transition. Cestari, *et al.* [6] performed an extensive study of CB7CB and revealed that, in spite of exhibiting smectic like defects, the N_{tb} phase was devoid of smectic order. Furthermore, their data suggested that the N-N_{tb} phase transition was near a tricritical point due to a coupling between the nematic and heliconical order parameters. Experiments showed that the heat capacity critical exponent was 0.5 consistent with tricritical behavior. The tricritical nature was further confirmed [9] by adiabatic calorimetric studies of the mixtures of the bimesogens (CB7CB) and a monomer nematic 4-pentyl-4'-cyanobiphenyl (5CB).

Freeze fracture transmission electron microscopy (FFTEM) studies [10,11] of two compounds have revealed a periodicity of ~ 8-9 *nm* in the N_{tb} phase of calamitic bimesogens. Gorecka, *et al.* [12], found a similar periodicity using atomic force microscopy (AFM) and suggested that surface freezing might explain the periodicity. Very recently, Zhu, *et al.* [13], used resonant soft x-ray scattering to show that there is a spatial periodicity of this length without electron density modulation. This is consistent with small-angle x-ray scattering experiments where no evidence of periodicity has been found in spite of several very diligent efforts [11, 14] and the appearance of smectic–like defects in the N_{tb} phase.

In order to gain further insight into the molecular organization in the N_{tb} phase and the nature of the N-N_{tb} transition we investigated CB7CB using x-ray diffraction (XRD) and polarized

Raman spectroscopy (PRS) to measure the orientational order parameters $\langle P_2(\cos\beta)\rangle$ and $\langle P_4(\cos\beta)\rangle$, the Legendre polynomials of order 2 and 4, respectively, and β is the polar angle measured from the director **n** (Fig. 1a), across the N-N_{tb} transition. These order parameters suggest a truncated conical (or, volcano-like [15]) molecular orientational distribution function (ODF) in the N_{tb} phase and allow a direct estimation of its cone angle, the main order parameter of the N_{tb} phase. The x-ray results are in good agreement with previously reported [16] values from optical birefringence.

XRD measurements were made on CB7CB flame-sealed in 1.5 mm diameter quartz capillaries placed in an in-situ magnetic field of ~2.5 kG produced by a pair of rare-earth permanent magnets mounted inside an INSTEC HS402 hot stage. X-ray experiments were performed at beamline X27C of the National Synchrotron Light Source (NSLS) using 1.371 Å x-rays and a MAR CCD detector (resolution 160×160 μm^2) placed at ~222.4 *mm* from the sample. The data were calibrated against silver behenate and silicon standards traceable to the National Institute of Standards and Technology. Background scattering was recorded with an empty capillary and subtracted from sample scattering, and data analyzed using FIT2D software [17].

The polarized Raman spectra were obtained using a 10 μm thick commercial quartz cell [18] with planar alignment. A Kaiser Raman System with a polarized 785nm laser was used to study the material (See *Appendix* for experimental details). The sample, mounted on a heating stage, was rotated by an angle θ and two sets of Raman spectra recorded with the polarizer parallel, $I_{\parallel}(\theta)$, and perpendicular, $I_{\perp}(\theta)$ to the analyzer. The Raman peak centered at 1605 cm^{-1} corresponding to the stretching of the benzene rings was analyzed to obtain the depolarization

ratio $R(\theta) = \frac{I_{\perp}(\theta)}{I_{\parallel}(\theta)}$. The method of Jones, *et al*., [19] was employed to obtain $\langle P_2(\cos\beta)\rangle$ and $\langle P_4(\cos\beta)\rangle$ by fitting $R(\theta)$The bend angle 122° of CB7CB molecule is taken into account in the fitting function introduced by Gleeson group [20]. This method has been successfully applied to the $\langle P_2(\cos\beta)\rangle$ and $\langle P_4(\cos\beta)\rangle$ measurements for both thermotropic and lyotropic liquid crystals [21].

In the N phase, the x-ray diffraction patterns consist of two pairs of orthogonal diffuse crescents, one at small angles (~ 12 Å) and the other in the wide-angle region (~ 4.45 Å) as previously reported [6]. The temperature dependence of the effective length scale obtained from the diffuse small angle peaks show a small discontinuity at the N-N_{tb} transition consistent with a weakly first order transition. The lack of sharp small angle peaks confirms an absence of smectic-like layering. The value 12Å was about half of the bimesogen's length (26 Å), showed no evolution with temperature, and will be discussed in another publication [22]. In contrast, the lateral length scale shows a continuous evolution.

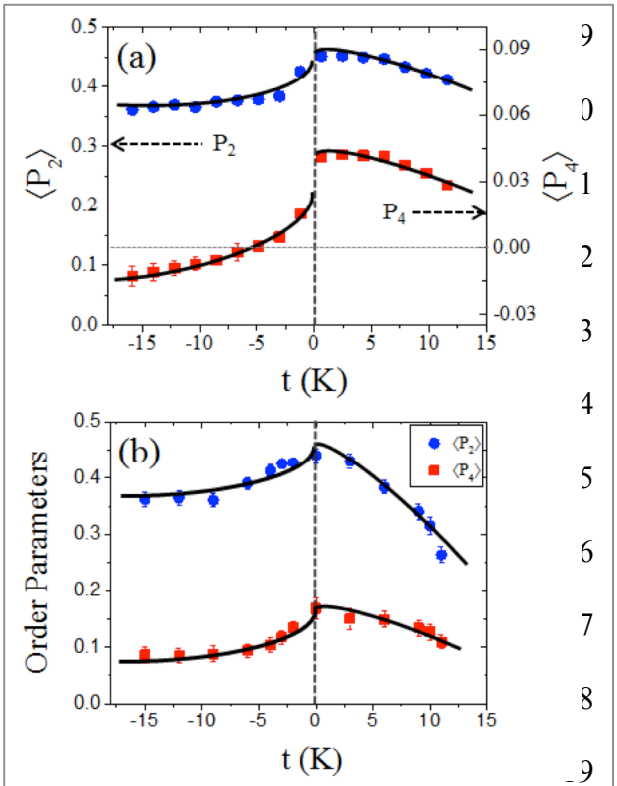

Figure 2: (color online) Temperature dependence of $\langle P_2(\cos\beta)\rangle$ and $\langle P_4(\cos\beta)\rangle$ in the nematic phases of CB7CB. (a) is XRD taken at NSLS, (b) is PRS. The lines are to guide the eye.

The line shape of the wide-angle x-ray reflections was analyzed to calculate [23] the

nematic orientational order parameters $\langle P_2(\cos\beta)\rangle$, $\langle P_4(\cos\beta)\rangle$, and $\langle P_6(\cos\beta)\rangle$ using the numerical inversion method of Davidson, *et al.* [24], Jenz, *et al.* [25] performed simulations to test the validity of this techniques and found that it slightly underestimates $\langle P_2\rangle$ by about 0.05, well below the experimental uncertainties. $\langle P_6\rangle$ was nearly zero in all cases and setting it equal to zero had no effect on the other order parameters. The temperature dependence of the two order parameters for CB7CB samples calculated from the XRD and PRS methods are shown in Fig. 2. The $\langle P_2\rangle$ values for both techniques are very similar. In the N phase, $\langle P_2\rangle$ is positive and increases from ~ 0.30 to 0.45 as the temperature is lowered. The probable error in values of $\langle P_2\rangle$ obtained from x-ray varies from ±0.02 (i.e., comparable to the size of the symbols) to ±0.03 (shown by error bars). The uncertainties are somewhat larger, typically ~ ±0.035 for the PRS method. They are larger for $\langle P_4\rangle$ as shown in Fig. 2. The values of $\langle P_2\rangle$ in the N_{tb} phase are in agreement with those obtained [26] from the ^{13}C 2D NMR technique. After a

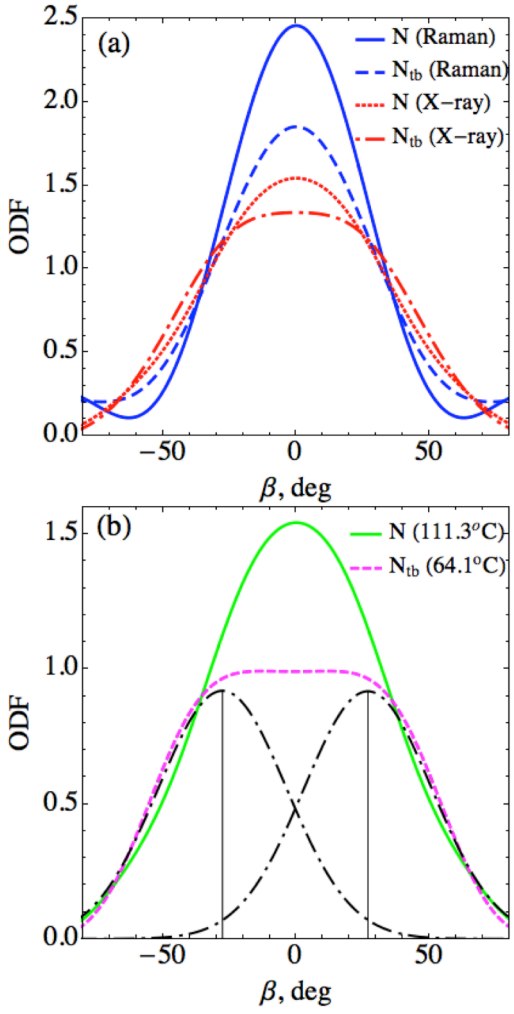

Figure 3: (Color online) (a) Orientational distribution functions in the N (t = 0 K) from Raman (blue solid line) and X-ray (red dotted line) and N_{tb} phases (t = -15 K) from Raman (blue dashed line) and X-ray (red dot-dashed line) of CB7CB. (b) The ODF in the N phase (green solid line) is sugarloaf-like but its shape changes to diffuse-cone (dashed magenta line) in the N_{tb} phase. The two black (dash-dot) curves are Gaussians fitted to the N_{tb} ODF. The separation between their centers, marked by solid vertical lines, is a measure of the cone/tilt angle.

significant initial drop in their values at the N - N_{tb} transition, $\langle P_2 \rangle$ continued to decrease and appear to flatten out at the lowest temperatures.

The $\langle P_4 \rangle$ obtained by the two techniques are different. This discrepancy of $\langle P_4 \rangle$ values is quite usual and has been systematically discussed in literature [27]. The $\langle P_4 \rangle$ obtained via PRS is systematically larger by about 0.1 than that obtained from XRD analysis. This is because XRD effectively probes the full dimer molecule whereas PRS probes the rigid part of the molecule. In spite of this they show similar thermal evolution. $\langle P_4 \rangle$ increases by a small amount with decreasing temperature in the N phase followed by a discontinuous decrease at the transition and then a non-linear decrease of approximately 0.04 for both XRD and PRS over a 15^{o}C decrease in temperature. The difference between the $\langle P_4 \rangle$ values obtained from our PRS measurements and those of reference [20] is barely discernable. In the N phase our $\langle P_4 \rangle$ values range from 0.1 to 0.18 while ref. [20] range from 0.15 to 0.20. The data point $\langle P_4 \rangle$ = 0.1 from our measurements lies very close to the nematic-isotropic transition. The slight difference between the values over the rest of the N phase is expected and understandable considering that the degree of alignment of the LC molecules in different sample cell cannot be exactly the same and is dependent on a number of factors such as the alignment layer used, degree of rubbing, etc. Furthermore, these values lie within the expected experimental uncertainties.

In the N_{TB} phase, our values decrease with decreasing temperature from 0.2 to 0.15. No comparison can be made with the results in ref. [20] as their only data point is in the vicinity of the N-N_{TB} transition because they were unable to uniformly align the dimer molecules on further cooling. We were able to obtain a more uniform alignment throughout the N_{TB} phase, by using a thinner cell also employed in reference [16] and discussed in the *Appendix*. The truncated

orientation distribution functions based on the $\langle P_2 \rangle$ and $\langle P_4 \rangle$ values from PRS (determined from the sum of Legendre polynomials [19,28] and XRD (directly obtained from the experimental azimuthal intensity distribution) are shown in Fig. 3a. The ODFs obtained from the two approaches are somewhat different as they probe the system differently; both PRS and XRD results show that the ODF is wider in the N_{tb} phase than it is in the N phase. Since the fluctuations of the molecules can only monotonically decrease with temperature, we believe the wider ODF is intrinsic to the N_{tb} phase. The ODFs in the N phase, where both order parameters are positive, are sugarloaf like and well approximated by a single Gaussian. However, it develops a flattened conical (or, volcano-like) shape in the N_{tb} phase providing direct evidence of conical distribution of the local director as previously predicted [29]. This is shown in Fig. 3b. The relative uncertainty in the shape of the ODF in the N_{tb} phase is reflected in the error bars of the orientational order parameters (Fig. 2) which ranges from 0.02 – 0.03 and 0.035 – 0.04 for x-ray and Raman values, respectively. Thus, the reliability of the derived ODF is high very good. We are unable to compare their reliability with others results, as there are no other reports of experimentally derived ODFs. These ODF plots represent a cross-section of the distribution in a plane containing the axis of the cone (i.e., the helix), and the two high points on the ODF depend on the tilt angle α of the local director (Fig. 1c) with respect to the global director $\boldsymbol{\mathcal{N}}$, or the cone axis. We measured α by fitting a sum of two Gaussians shown by dot-dash curves in Fig. 3b, to the ODF at different temperatures in the N_{tb} phase. The angle α is one half of the separation between the centers of the Gaussians, and is plotted in Fig. 4 as a function of $t^* = T^* - T$, where T^* is the temperature at which $\alpha = 0$ in a power law fit and represents the extrapolated second order transition temperature. A typical uncertainty in α is $\pm 0.2^o$. The tilt angle extrapolates to zero at $T^* = T_{Ntb\text{-}N} + 1.7$ K and attains a maximum value of about 24° ~15K into the N_{tb} phase. The

temperature dependence of the tilt angle fits well to a simple power law: $\alpha(T) \propto (T^* - T)^{\lambda}$ with $\lambda = 0.19 \pm 0.03$. The closeness of T^* to $T_{Ntb\text{-}N}$ is indicative of a weakly first-order phase transition [30]. Since the cone angle is the main order parameter of the N_{tb} phase, an exponent of 0.25 for tricritical or 0.5 for the mean-field behavior is expected. Our value is close to that expected for tricritical behavior. The difference is not surprising because the transition in these materials has been shown to be weakly first order [16] and more data points near the N-N_{tb} transition and a better measurement of $T_{Ntb\text{-}N}$ are necessary to make conclusive statements about the critical exponent.

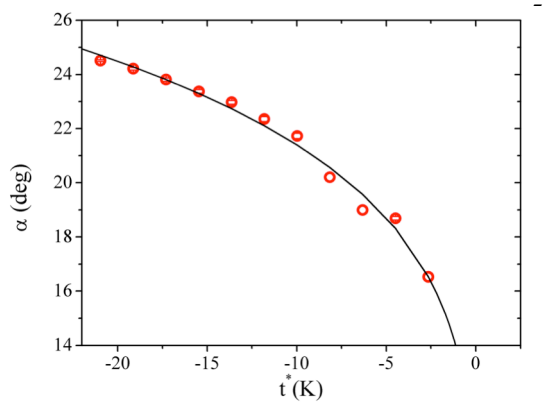

Figure 4: The heliconical tilt angle α in the N_{tb} phase of CB7CB as a function of $t^* = T^* - T$, where T^* is the temperature at which $\alpha = 0$. The curve is a single power law fit.

To conclude, the temperature dependence of the orientational order parameters $\langle P_2 \rangle$ and $\langle P_4 \rangle$ has been measured in the N and N_{tb} phases of CB7CB. X-rays that measure an average electron density order parameter obtain a negative value of $\langle P_4 \rangle$ in the N_{tb} phase; thus, confirming a conical local director configuration in this phase. However, Raman scattering that measures a given vibration of the molecule finds a $\langle P_4 \rangle$ with a similar temperature dependence, but systematically larger by approximately 0.1; such behavior is expected [16] and should be anticipated. The measured $\langle P_2 \rangle$ of both techniques are in very good agreement in the N_{tb} phase. The ODF has a sugarloaf shape in the N phase that becomes volcano-like in the N_{tb} phase. Thermal evolution of the cone angle, directly measured via the XRD ODF, is qualitatively in good agreement with previously reported optical values, and exhibits simple power law behavior The tilt angle measured at molecular length scale should determine the macroscopic optical

properties of the N_{tb} phase. So, an agreement between the values of α obtained from XRD and optical methods is expected.

ACKNOWLEDGEMENTS

This work was supported by the Basic Energy Science program of the Office of Science, Department of Energy award SC-0001412. The synthesis work of J.-K. S. was supported by the National Research Foundation of Korea (NRF) grant funded by MSIP (No. 2014R1A2A1A11054392).

Appendix: POLARIZED RAMAN SPECTROSCOPY (PRS)

We employed a *Kaiser* Raman System to perform the Polarized Raman spectra measurements. The CB7CB was sandwiched between two quartz plates separated by 10 μm- thick spacer (*Instec Inc*). A polarized 785 nm laser beam is focused on to the aligned CB7CB via a 50× microscope objective (NA = 0.55). By rotating the sample mounted on a heating stage, two sets of the Raman spectra one with the polarizer parallel and the other perpendicular to the analyzer (e.g. Fig. A1 (a) and (b)) in a wide range of temperature (65 ˚C~120 ˚C) were obtained. The peaks centered at 1605 cm^{-1} that correspond to the stretching of the benzene ring were fit, and a plot the peak height as function of the sample rotation angle are shown in Figs. A1 (c) and (d).

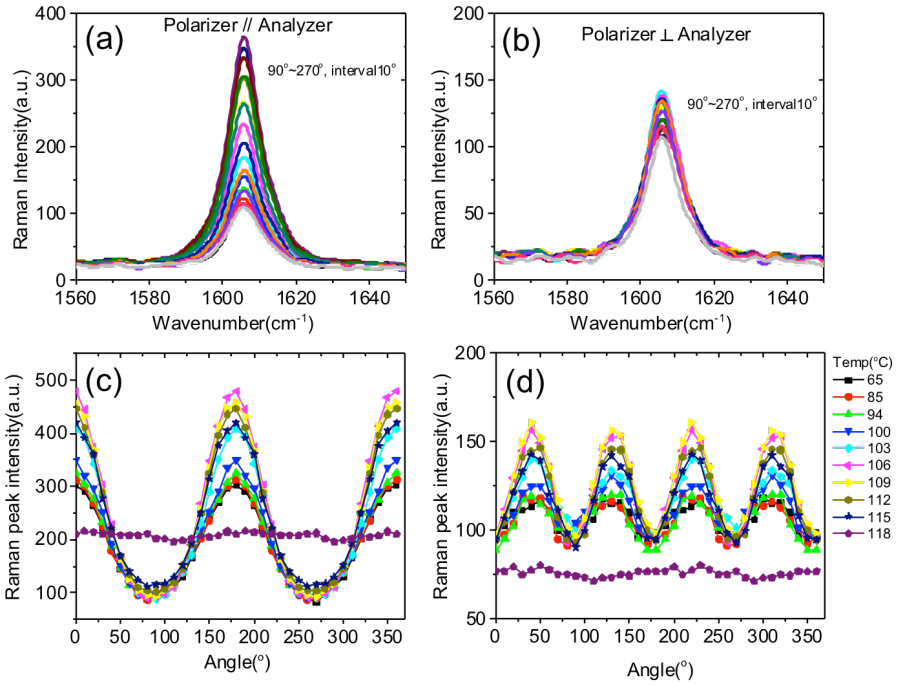

Fig. A1: Raman spectra shown in (a) and (b), and peak intensities shown in (c) and (d) at different temperatures.

From these measurements, the Raman depolarization ratio defined as $R(\theta) = I_{\perp}(\theta)/I_{//}(\theta)$, with θ the angle between the LC director and the polarization of the excitation laser is obtained.

Theoretically $R(\theta)$ can be expressed in terms of the order parameters as,

$$R(\theta) = \frac{(-1+r)^2\begin{Bmatrix} -40\langle P_{200}\rangle - 240\langle P_{220}\rangle \\ +(105\cos 4\theta - 9)\langle P_{400}\rangle \\ -2\left[28+90(1+7\cos 4\theta)\langle P_{420}\rangle + 210\sin^2 2\theta\langle P_{440}\rangle\right] \end{Bmatrix}}{\begin{Bmatrix} 40(4r^2-r-3)[(1+3\cos 2\theta)\langle P_{200}\rangle + 12\sin^2\theta\langle P_{220}\rangle] \\ -3(r-1)^2(9+20\cos 2\theta + 35\cos 4\theta)\langle P_{400}\rangle \\ -8[7(3+4r+8r^2)+30(r-1)^2\sin^2\theta(3(5+7\cos 2\theta)\langle P_{420}\rangle + 7\sin^2\theta\langle P_{440}\rangle)] \end{Bmatrix}} \quad \text{(A1)}$$

Using the experimental data in Fig. A1, all the parameters in Eq. (A1) can be extracted by fitting the $R(\theta)$ curve. In principle, Raman spectroscopy can provide directional information up to the 4th rank directional information. However, there will be too much freedom using six free parameters to fit the $R(\theta)$. Hence we first include only the uniaxial order parameters for the

fitting of $\langle P_{200} \rangle$, $\langle P_{400} \rangle$ and 'r', the differential polarizability ratio. Under this approximation, the expression (A1) reduces to,

$$R(\theta) = \frac{(r-1)^2[56+40\langle P_{200}\rangle+(9-105\cos 4\theta)\langle P_{400}\rangle]}{\left[\begin{matrix}56(8r^2+4r+3)-40(4r^2-r-3)(1+3\cos 2\theta)\langle P_{200}\rangle \\ +3(r-1)^2(9+20\cos 2\theta+35\cos 4\theta)\langle P_{400}\rangle\end{matrix}\right]} \quad \text{(A2)}$$

Using Eq. (A2), we obtain the order parameters of CB7CB for each temperature as shown in Fig. 2 (b) in the manuscript.

In the N_{TB} phase, LC alignment is easily lost on further cooling making it difficult to make the measurements. To circumvent this difficulty, we performed the measurement on a 10 μm cell with a cooling rate of 4°/min. There are still "parabolic defects", but the aligned dark areas are dominant, as shown in Fig. A2 under cross polarizers. With a 50× (NA = 0.5) objective lens, the laser beam may be focused to a diameter as small as 5 μm. Since a typical domain is ~50 μm in size precise measurements on one of the aligned domains are obtained.

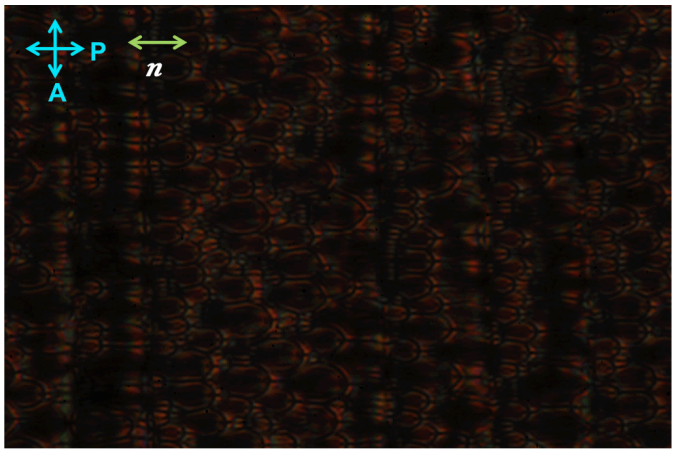

Fig. A2: Optical texture of CB7CB in the N_{tb} phase.

REFERENCES:

[1] S. Kumar, *Liquid Crystals: Experimental Study of Physical Properties and Phase Transitions* (Cambridge University Press, Cambridge, 2002).

[2] I. Dozov, Europhys. Lett. **56**, 247 (2001).

[3] R. Memmer, Liq. Cryst. **29**, 483 (2002).

[4] V. P. Panov, M. Nagaraj, J. K. Vij, Y. P. Panarin, A. Kohlmeier, M. –G. Tamba, R. A. Lewis, and G. H. Mehl, Phys. Rev. Lett. **105**, 167801 (2010).

[5] P. A. Henderson and C. T. Imrie, Liq. Cryst. **38**, 1407 (2011).

[6] M. Cestari, S. Diez-Berart, D. A. Dunmur, A. Ferrarini, M. R. de la Fuente, D. J. B. Jackson, D. O. Lopez, G. R. Luckhurst, M. A. Perez-Jubindo, R. M. Richardson, J. Salud, B. A. Timimi, and H. Zimmermann, Phys. Rev. E 84, 031704 (2011).

[7] D. Chen, M. Nakata, R. Shao, M. R. Tuchband, M. Shuai, U. Baumeister, W. Weissflog, D. M. Walba, M. A. Glaser, J. E. Maclennan, and N. A. Clark, Physical Review E **89**, 022506 (2014).

[8] Y. Wang, G. Singh, D. M. Agra-Kooijman, M. Gao, H. K. Bisoyi, C. Xue, M. R. Fisch, S. Kumar, and Q. Li, CrystEngComm **17**, 2778 (2015).

[9] C. Tripathi, P. Losada-Pérez, C. Glorieux, A. Kohlmeier, M.-G.Tamba, and G. H. Mehl, J. Leys, Physical Review E **84**, 041707 (2011).

[10] V. Borshch, Y. K. Kim, J. Xiang, M. Gao, A. Jákli, V. P. Panov, J. K. Vij, C. T. Imrie, M. G. Tamba, G. H. Mehl, and O. D. Lavrentovich, Nat. Commun. **4**, 2635 (2013).

[11] D. Chen, J. H. Porada, J. B. Hooper, A. Klittnick, Y. Shen, M. R. Tuchband, M. R Proc. Natl. Acad. Sci. U. S. A. **110**, 15931 (2013).

[12] E. Gorecka, M. Salamonczyka, A. Zepa, D. Pociechaa, C. Welch, Z. Ahmed, and G. H. Mehl, Liq. Cryst., **42**, 1 (2015).

[13] C. Zhu, M. R. Tuchband, A. Young, M. Shuai, A. Scarbrough, D. M. Walba, J. E. Maclennan, C. Wang, A. Hexemer, and N. A. Clark, Physical Review Letters **116**, 147803 (2016).

[14] K. Adlem, M. Copic, G. R. Luckhurst, A. Mertelj, O. Parri, R. M. Richardson, B. D. Snow, B. A. Timimi, R. P. Tuffin, and D. Wilkes, Physical Review. E **88**, 022503 (2013).

[15] S. T. Lagerwall, P. Rudquist, and F. Giesselmann, Mol. Cryst. Liq. Cryst. **510**, 148 (2009).

[16] C. Meyer, G. R. Luckhurst, and I. Dozov, J. Mater. Chem. C **3**, 318 (2015).

[17] A. P. Hammersley, S. O. Svensson, M. Hanfland, A. N. Fitch, and D. Hausermann, High Pressure Res. **14**, 235 (1996).

[18] Instec, Inc. (http://www.instec.com/)

[19] (a) W. J. Jones, D. K. Thomas, D. W. Thomas, and G. Williams, J. Mol. Struct. **708**, 145 (2004).

[20] Z. Zhang, V. P. Panov, M. Nagaraj, R. J. Mandle, J. W. Goodby, G. R. Luckhurst, J. C. Jones, and H. F. Gleeson, J. Mater. Chem. C **3**, 10007 (2015).

[21] M. S. Amer, *Raman spectroscopy for soft matter applications* (Wiley, Hoboken, N.J., 2009).

[22] D. M. Agra-Kooijman *et al.* (unpublished).

[23] D. M. Agra-Kooijman, H. G. Yoon, S. Dey, and S. Kumar, Physical Review E **89**, 032506 (2014).
[24] P. Davidson, D. Petermann, and A. Levelut, J. Phys. II (France) **5**, 113 (1995).
[25] F. Jenz, S. Jagiella, M. A. Glasser, and F. Giesselman, ChemPhysChem **17**, 1568 (2016).
[26] J. W. Emsley, M. Lelli, A. Lesage, and G. R. Luckhurst, J. Phys. Chem. B **117**, 6547 (2013).
[27] A. Sanchez-Castillo, M. A. Osipov, and F. Giesselmann, Phys. Rev E **81**, 021707 (2010).
[28] M. S. Park, Y. S. Wong, J. O. Park, S.S. Venkatraman and M. Srinivasarao, Macromolecules, **44**, 2120 (2011).
[29] M. Osipov and G. Pajak, Phys. Rev. E **85**, 021701 (2012).
[30] E. F. Gramsbergen, L. Longa, and Wim H. de Jeu, Physics Reports, **135**, 195-257 (1986).